AD_____

AWARD NUMBER DAMD17-97-1-7190

TITLE: The Design and Emulation of a Multiple-Camera SPECT Breast Imager

PRINCIPAL INVESTIGATOR: John D. Sain

CONTRACTING ORGANIZATION: University of Arizona
Tucson, Arizona 85722-3308

REPORT DATE: June 1998

TYPE OF REPORT: Annual

PREPARED FOR: Commander
U.S. Army Medical Research and Materiel Command
Fort Detrick, Maryland 21702-5012

REPORT DOCUMENTATION PAGE

Form Approved
OMB No. 0704-0188

1. AGENCY USE ONLY *(Leave blank)*	2. REPORT DATE	3. REPORT TYPE AND DATES COVERED
	June 1998	Annual (19 May 97 - 18 May 98)

4. TITLE AND SUBTITLE

The Design and Emulation of a Multiple-Camera SPECT Breast Imager

5. FUNDING NUMBERS

DAMD17-97-1-7190

6. AUTHOR(S)

John D. Sain

7. PERFORMING ORGANIZATION NAME(S) AND ADDRESS(ES)

University of Arizona
Tucson, Arizona 87522-3308

8. PERFORMING ORGANIZATION REPORT NUMBER

9. SPONSORING / MONITORING AGENCY NAME(S) AND ADDRESS(ES)

U.S. Army Medical Research And Materiel Command
ATTN: MCMR-RMI-S
504 Scott Street
Fort Detrick, Maryland 21702-5012

10. SPONSORING / MONITORING AGENCY REPORT NUMBER

11. SUPPLEMENTARY NOTES

12a. DISTRIBUTION / AVAILABILITY STATEMENT

Approved for public release; distribution unlimited

12b. DISTRIBUTION CODE

13. ABSTRACT *(Maximum 200 words)*

This report summarizes the work completed in Year 1 of this grant. The work included characterizing radioactivity within the breast, building phantoms for imaging, modeling the detector response, and optimizing the imaging system geometry.

Standard clinical injections of Tc-99m Sestamibi contain 20 mCi of activity. The estimated percentage of the activity taken up by a single breast of average mass is about 0.08 %, which corresponds to about 16 uCi. The estimated activity per unit mass of normal breast tissue is 43 dpm/mg. The uptake of Tc-99m Sestamibi in abnormal breast tissues (relative to normal tissue) was examined. The degree of uptake varied significantly with the histological type (not grade) of malignant tumors. Ductal and lobular carcinomas exhibited relative uptake ratios of nearly 6:1, fibroadenomas nearly 3:1, and fat and benign tumors about 1:1. Phantoms of breasts with lesions and a torso with heart and liver were constructed. The mean responses of the small and large modular cameras were characterized. An optical model, providing estimates of the camera response to gamma rays incident anywhere on the camera face, was developed. The locations and fields of view of the small cameras were modified to partially optimization the imaging system geometry. (196)

14. SUBJECT TERMS

Breast Cancer

mammoscintigraphy,SPECT,modular gamma camera,technetium-99m

15. NUMBER OF PAGES 28

16. PRICE CODE

17. SECURITY CLASSIFICATION OF REPORT	18. SECURITY CLASSIFICATION OF THIS PAGE	19. SECURITY CLASSIFICATION OF ABSTRACT	20. LIMITATION OF ABSTRACT
Unclassified	Unclassified	Unclassified	Unlimited

FOREWORD

Opinions, interpretations, conclusions and recommendations are those of the author and are not necessarily endorsed by the U.S. Army.

____ Where copyrighted material is quoted, permission has been obtained to use such material.

____ Where material from documents designated for limited distribution is quoted, permission has been obtained to use the material.

JDS Citations of commercial organizations and trade names in this report do not constitute an official Department of Army endorsement or approval of the products or services of these organizations.

____ In conducting research using animals, the investigator(s) adhered to the "Guide for the Care and Use of Laboratory Animals," prepared by the Committee on Care and Use of Laboratory Animals of the Institute of Laboratory Resources, National Research Council (NIH Publication No. 86-23, Revised 1985).

____ For the protection of human subjects, the investigator(s) adhered to policies of applicable Federal Law 45 CFR 46.

____ In conducting research utilizing recombinant DNA technology, the investigator(s) adhered to current guidelines promulgated by the National Institutes of Health.

____ In the conduct of research utilizing recombinant DNA, the investigator(s) adhered to the NIH Guidelines for Research Involving Recombinant DNA Molecules.

____ In the conduct of research involving hazardous organisms, the investigator(s) adhered to the CDC-NIH Guide for Biosafety in Microbiological and Biomedical Laboratories.

John D. Sain 5-20-98

PI Signature Date

TABLE OF CONTENTS

INTRODUCTION

This report contains a description and summary of the work completed in Year 1 of the three-year grant entitled "The Design and Emulation of a Multiple-Camera SPECT Breast Imager". The purpose of the research in Year 1 was to create a realistic model of a human breast and torso that would serve as the object to be imaged, to characterize the scintillation cameras that are the system detectors, and to optimize the overall geometry of the system. In other words, the purpose of the research was to set up and characterize the basic components of the imaging system.

Specifically, in Year 1 of this grant, the principal investigator was to work on five tasks. (1) Given a female patient in the clinic who had been injected with Tc-99m Sestamibi, what percentage of the injected activity ended up in a single breast as a function of breast mass? Also, what was the relative uptake of Tc-99m Sestamibi in different types of abnormal breast tissues (i.e. tumors)? (2) Phantoms of a human breast and the adjacent chest cavity were to be built. The breast phantom was to include lesions (hot or cold) which could be placed inside at any location. The torso phantom was to provide realistic background activity for the breast. (3) The mean response of the small modular gamma cameras was to be characterized. The actual mean response of a small camera is well known since many have been calibrated in the laboratory. An optical model (in software) was to be developed to estimate the mean response and then incorporated into the system emulation. (4) The mean response of the large modular gamma camera was to be characterized. A camera of this type has not been built yet, so the mean response would have to be generated by a model which, once developed, would also be used in the emulation. (5) The basic geometry of the imaging system was to be optimized. In particular, the optimization was to include the position and field of view of the small cameras, the number, size, and arrangement of apertures for the small cameras, and the magnification of the object.

The main body of the report contains a full description of the work completed in each task.

OBJECTIVE 1

Task 1. Characterize the expected radiotracer activity within the breast.

The factors to be determined in this task were (1) the percentage of the original injected activity taken up by a single breast, depending on its size and whether it contains any abnormalities, and (2) the relative uptake of Tc-99m Sestamibi in different types of breast tissue.

Two minor changes, however, were made to the sub-tasks. First, the estimated activity per unit mass of normal tissue in units of decays per minute per milligram (dpm/mg) is a very useful quantity. Given a breast mass, the percentage of the original injected activity taken up by the breast can be directly found. So instead of reporting the percentage of the original injected activity taken up by a single breast as a function of size, it seemed more reasonable to report the estimated activity per unit mass of tissue and, as a reference, the percentage of the original injected activity taken up by a single breast of average mass. Second, the original purpose of the second subtask was to determine the relative uptake of Tc-99m Sestamibi in different types of abnormal breast tissue. Consideration of abnormalities in the first subtask leads to unnecessary redundancy.

Thus, the factors actually determined in this task were (1) the percentage of the original injected activity taken up by a single normal breast of average mass, and (2) the relative uptake of Tc-99m in different types of abnormal breast tissue.

Recent research involving mammoscintigraphy has provided many new insights into the relative uptake of radiotracers by various types of tissue within the human breast. A common approach is to report the tumor-to-background ratio (TBR) of the lesion under study along with its size and histological type and grade. Few studies to date, however, have measured the absolute uptake of radiotracer within the tissues themselves. This is due in part to the fact that in situ measurements are, for obvious reasons, unrealistic, so the study protocol would have to include surgical removal of tissue samples.

In order to estimate the percentage of the original injected activity taken up by a normal breast, it would be convenient to know both the approximate mass of the breast and the approximate activity per unit mass in normal breast tissue. Estimating the mass of the breast is not difficult. Several models of the human body have been developed which assign masses to each organ and tissue group. The Cristy-Eckerman model[1], for example, a well-known model that will be used in this research, assigns a mass of 410 grams (g) to an average adult female breast. Estimating the activity per unit mass in normal breast tissue, however, is not as easy. Thus, three different approaches were utilized to complete this task. The first approach took advantage of a study which, as part of its protocol, surgically removed samples of breast tissue and measured the absolute activity in each case. The second approach used data from a study, which attempted to measure the biodistribution of several radiotracers within the human body. The third approach involved analyzing several breast images collected by a modular gamma camera dedicated to breast imaging. Each approach is described in more detail below.

The first approach used data from a study by Maublant *et al.*[2] which measured the accumulation of Tc-99m Sestamibi in breast tumors and corresponding lymph nodes in

patients scheduled for breast surgery. On the day before surgery, each patient underwent mammoscintigraphy with 20 mCi of Tc-99m Sestamibi. The next morning each patient was injected with 10 mCi of Tc-99m Sestamibi and underwent surgery. Immediately after surgery the weight and activity of each tissue sample was recorded before it underwent histological analysis. The activity of each sample was normalized to the mean activity of normal tissue samples obtained from the same patient. The study recorded the number of samples and average relative uptake for each histological classification of tissue (see Table 1). The overall average mass (562 mg) and average activity per unit mass (89 dpm/mg) of the tissue samples was also reported. Using this information, the average activity per unit mass of normal breast tissue was estimated to be 42.9 ± 1.8 dpm/mg. This estimate is comparable to the actual measured value[3] of 43.57 ± 35.67 dpm/mg. For an average breast mass of 410 g, this corresponds to 0.0792 % of the original injected activity.

The second approach used data from a study by Wackers *et al.*[4] which evaluated the biodistribution, dosimetry, and safety of Tc-99m Sestamibi in normal volunteers during both rest and exercise. Patients were injected with a known amount of radiotracer, and then upper body and whole body images were collected with a standard large field-of-view gamma camera at several specified postinjection times. Regions of interest were drawn on the images, and the percent of injected activity within various organs and parts of the body was estimated. Combining the data collected five minutes postinjection with the Cristy-Eckerman model[5] of the female body, the average activity per unit mass of normal breast tissue could be estimated. The estimated activity per unit mass of normal breast tissue was 259 ± 37 dpm/mg, and the percentage of original injected activity for an average mass breast was 0.478 %.

The third approach involved collecting images of breasts with a dedicated modular gamma camera in the Department of Nuclear Medicine here at University Medical Center. The camera, nicknamed SAMCAM ("Stand Alone Modular CAMera"), is an operating version of the "small" modular gamma camera referred to in the proposal for this grant. **(NOTE: The operation of SAMCAM was supported by another research grant that was fully approved for human studies.)** In each study the patient had been injected with 25 mCi of Tc-99m Sestamibi and undergone imaging on standard clinical instruments for other medical reasons. Upon completion of those studies, the patient volunteered to have one/both breasts imaged by SAMCAM. In each image the number of gamma rays, both primary and scatter, detected by the camera was recorded. Choosing the studies which appeared to involve medium-sized breasts and assuming, according to the Cristy-Eckerman model, that the average mass of the breasts was 410 g, the average activity per unit mass of normal breast tissue could be estimated. The average activity per unit mass of normal breast tissue in this case was 24.66 dpm/mg, and the corresponding percentage of original injected activity for an average mass breast was 0.0455 %.

In conclusion, the three methods generated estimates (42.9 ± 1.8 dpm/mg, 257 ± 37 dpm/mg, 24.66 dpm/mg) which were almost within the same order of magnitude. Given the diversity of the methods, it is encouraging that the three estimates are so close. The first method (the Maublant *et al.* study), however, is arguably the most accurate of the three due to the fact that the activity per unit mass of the normal tissue samples was actually measured. The second and third methods involved much larger amounts of uncertainty both in the data and the calculations. They merely provide some measure of

confirmation of the magnitude of the estimated quantity. Thus, the estimated activity per unit mass of normal tissue is roughly 43 dpm/mg, and the estimated percentage of the original injected activity taken up by a single breast of average mass is about 0.08 %.

The second part of this task was to determine the relative uptake of Tc-99m Sestamibi in different types of abnormal breast tissue. The uptake of a radiotracer by tissues in the human body is a complex process. Different types of tissues -- such as normal, fatty, scar, diseased, and cancerous -- exhibit varying degrees of uptake which, in turn, can be affected by different characteristics of the tissue -- such as size, metabolism, and vascularity. In the case of Tc-99m Sestamibi in breast tissue, the uptake process is still not completely understood at the biological level. It has been well established, however, that malignant breast tumors readily take up Tc-99m Sestamibi. So recent research has focused, in part, on trying to determine the relative uptake of Tc-99m Sestamibi by different types of breast tissue. Then the medical community will know what types of abnormalities are readily visualized by this particular radiotracer.

This problem can be examined from several points of view. The first point of view is that of "internal data" -- measurements of activity made on surgically extracted tissue samples. The second point of view is that of "external data" -- measurements of the tumor-to-background ratio which have been calculated from scintigraphic images. The third point of view is that of "error-rate data" -- looking at data on TP/FP/TN/FN's and noting which types of tissues are typically associated with each category.

Looking at the first point of view, at least one study has measured the absolute activity of Tc-99m Sestamibi in surgically extracted tissue samples.

The study by Maublant *et al.* was motivated, in part, by the authors' belief that mammoscintigraphy with Tc-99m Sestamibi could provide help with evaluating breast tumors, but the actual concentration of the radiotracer in the tumor tissue was unknown. The authors wanted to know whether false-negative results in imaging were due to a lack of radiotracer uptake by the malignant tumor or due to physical limitations of the scintillation cameras. The tissue samples were classified into seven groups according to histological analysis, and an average relative uptake was determined for each group (see Table 1). Note that the relative uptake is significantly higher in the "carcinoma only" samples which were either ductal or lobular carcinoma. The "carcinoma with fat or breast

Table 1. Relative uptake as a function of histological type (Maublant *et al.)*.

Histological classification	*Number of samples*	*Relative uptake*
normal breast and fat tissue	34	1.00 ± 0.22
noninvaded lymph nodes with fat tissue	14	1.31 ± 0.73
noninvaded lymph nodes only	111	1.80 ± 0.79
invaded lymph nodes with fat tissue	7	2.01 ± 0.83
invaded lymph nodes only	1	5.35
carcinoma with fat or breast tissue	5	1.40 ± 0.26
carcinoma only	22	5.64 ± 3.06

tissue" samples were not histologically pure and contained a mixture of normal breast and/or fat tissue with tumor cells. Thus, the relative uptake is much lower. Also noteworthy was that the mean relative uptake was 2.83 ± 0.81 in the four samples corresponding to fibroadenoma. Since the distribution of relative uptake was much wider in the "carcinoma only" group than in the others, the authors attempted to isolate factors that could account for the spread. One factor was that the normal tissue samples used to establish the relative uptake in each patient were composed of either fat or a mixture of fat and breast tissue. A difference between these two subgroups could have biased the relative uptake calculations. No significant difference existed, however, between tumor uptake relative to fat tissue (6.13 ± 2.37) and tumor uptake relative to a mixture of breast and fat tissue (5.09 ± 3.88). Another factor was the elapsed time between injection of radiotracer and surgical removal of samples, during which the radiotracer distribution may have changed. No correlation existed. Another factor was physical/biological characteristics of the patients. Only a weak correlation with body weight was found. Finally, the tumor contrast uptake was significantly correlated with the scintimammographic score but not with histological grade. The authors concluded that malignant breast tumors (ductal and lobular carcinomas in this case) take up nearly six times as much Tc-99m Sestamibi as the surrounding normal breast or fat tissue.

Looking at the second point of view, many studies have measured the tumor-to-background ratio in scintigraphic images.

A study by Ambrus *et al.*[6] demonstrated that malignant tumors took up more Tc-99m Sestamibi than surrounding normal tissue. The TBR's for both benign tumors and various stages of malignant tumors (according to the Bloom and Richardson classification scheme) are summarized in Table 2. The uptake of radiotracer is greater in the malignant tumors and among them the most advanced grade exhibits the highest uptake. Other studies, however, have indicated those greater uptakes by advanced grades of cancer are

Table 2. Average TBR as a function of histological grade (Ambrus *et al.*).

Histological grade[7]	*Average TBR*
1	1.37
2	1.29
3	1.71
benign	1.05

not due primarily to the histological grade but rather the histological type of the tumor. Ductal carcinomas, which are known to exhibit higher uptakes than other types of cancers, comprised 33 of the 40 malignant tumors in this study. Thus, the high TBR for grade 3 malignancies in this study may possibly be explained by the large percentage of ductal carcinomas in that classification grade.

A study by Mangkharak *et al.*[8] on palpable lesions found that malignant lesions, particularly those of advanced histological grade, demonstrated higher uptake of Tc-99m Sestamibi. Table 3 lists the average TBR as a function of histological grade (according to

Table 3. Average TBR as a function of histological grade (Mangkharak *et al.*).

Histological grade[9]	*Average TBR*
2A	1.57 ± 0.48
2B	1.53 ± 0.37
3A	2.30 ± 0.36
3B	2.93 ± 1.28
4	2.12 ± 0.38

the TNM system of the American Joint Committee on Cancer). In this study the mean uptake tended to increase from stage 2B to stage 3B but not in stage 4.

A study by Buscombe *et al.*[10] concluded that the histological grade of ductal carcinoma had no significant effect on the uptake of Tc-99m Sestamibi. As shown in Table 4, no significant difference exists in the average TBR's for different grades of cancer. The

Table 4. Average TBR as a function of histological grade (Buscombe *et al.*).

Bloom Richardson grade	*Average TBR*
1, 2	2.10 ± 0.65
3	1.95 ± 0.62

authors also considered other factors that they figured might affect the uptake. These factors included patient age (under/over 45 years), lesion diameter (under/over 20 mm), axillary disease (yes/no), and ductal type (yes/no). In each case, the difference in uptake was insignificant. Considering the factor of histological type, the study compared TBR's among ductal carcinomas, other types of cancers, and benign tumors. The data, listed in Table 5, indicates that ductal carcinomas exhibit a higher uptake of Tc-99m Sestamibi than

Table 5. Average TBR as a function of histological type (Buscombe *et al.*).

Histological type	*Average TBR*
ductal carcinoma	2.07
other cancers	1.31
benign tumors	1.46

other types of cancers as well as benign tumors. This suggests that the histological type, and not the histological grade, has a greater effect on the uptake of radiotracer.

A study by Chen *et al.*[11] reported a significant difference in uptake between malignant and benign tumors. The average TBR's, seen in Table 6, indicate that malignant tumors have a much higher uptake of radiotracer than the benign ones.

All of the studies just cited indicate that malignant tissues exhibit a higher uptake of Tc-99m Sestamibi than normal and fatty tissues and benign tumors. The tumor-to-background ratio appears to range from 1.5:1 to 3.0:1 with a concentration near 2.0:1. Among the various types of malignant tissues, ductal carcinoma appears to have the highest relative uptake.

Table 6. Average TBR as a function of tumor type (Chen *et al.*).

Tumor type	*Average TBR*
malignant	1.70 ± 0.53
benign	1.08 ± 0.23

Looking at the third point of view, several studies[12,13,14,15,16,17,18] have looked at clinical diagnoses of tumors and the corresponding pathological follow-ups.

True-positive (TP) results usually occur for carcinomas, the most common types of which are ductal and lobular. These malignant tumors typically exhibit a high rate of metabolism which leads to a higher uptake of Tc-99m Sestamibi. True-negative (TN) results can occur in the cases of inflammations (i.e. mastitis), cysts, fibrocystic disease, benign tumors (i.e. papilloma, fibroadenoma), and hyperplasia (i.e. epithelial hyperplasia). In these cases the abnormal growth of tissue is detectable on a mammogram but is not taking up a significant amount of radiotracer. False-positive (FP) results can occur for inflammations (i.e. mastitis), fibrocystic disease with and without epithelial hyperplasia, fibroadenomas, and sclerosing adenoses. In these cases not only is there abnormal tissue growth but the cells are also taking up a relatively large amount of Tc-99m Sestamibi. While the diagnosis at the time may be a false alarm for the patient, a biopsy is worthwhile because epithelial hyperplasia is associated with a two-fold risk for later development of carcinoma[19] as is sclerosing adenosis[20]. False-negative (FN) readings can occur for carcinomas of small dimensions, typically less than 1 cm, and microcalcification clusters. In the case of the carcinomas, the tumor may be taking up a significant amount of radiotracer for its size, but, due to its size or location within the breast, the cameras cannot detect it.

Thus, carcinomas usually exhibit a relatively high uptake of Tc-99m Sestamibi and, unless they are rather small (less than 1 mm in diameter), are easily detected. Tc-99m Sestamibi, however, is not taken up exclusively by malignant tumor cells. Various types of benign tissues -- whether just relatively large and/or just growing quickly -- have been shown to exhibit high uptakes of Tc-99m Sestamibi as well.

In conclusion, the three different approaches to determine the relative uptake of Tc-99m Sestamibi in different types of breast tissue led to similar results. The first approach, which measured the absolute activity of Tc-99m Sestamibi in surgically extracted tissue samples, concluded that Tc-99m Sestamibi strongly concentrates in malignant breast tumors (ductal and lobular carcinomas, in particular) with an average relative uptake ratio of nearly 6:1 compared with that of surrounding normal breast or fat tissue. The second approach, which measured the tumor-to-background ratio calculated from scintigraphic images, concluded that malignant tissues (ductal carcinoma, in particular) exhibit a higher uptake of Tc-99m Sestamibi than normal and fatty tissues and benign tumors. The tumor-to-background ratio ranged from 1.5:1 to 3.0:1 with a concentration near 2.0:1. The third approach, which looked at data on TP/FP/TN/FN's and noted which type of tissues are typically associated with each category, found that ductal and lobular carcinomas usually provided true-positive results if the lesions were not too small (less than 1 cm in diameter). The study also indicated that inflammations, fibrocystic disease, fibroadenomas, and sclerosing adenoses were capable of generating

false-positive results. Thus, all three approaches indicate that (1) ductal and lobular carcinoma exhibit abnormal tissue growth and relatively high uptakes of Tc-99m Sestamibi and (2) normal and fatty tissues exhibit relatively low uptakes of Tc-99m Sestamibi. Some other types of tissues, fibroadenomas, for example, are capable of exhibiting abnormal cell growth and relatively high uptake of radiotracer, but may not do so on a consistent basis.

Task 2. Build a realistic model of the human breast and adjacent chest wall.

A model of the female torso containing breast, heart, and liver phantoms has been built (see Figure 1). The original proposal, anticipating that imaging would be performed on an erect (standing or sitting) patient, called for a model of the breast and chest wall for an erect patient. The prone position, in which the patient lies horizontally on her stomach with pendant breasts, however, is proving to be a better position. Prone imaging of a single breast provides maximum separation of the breast tissue from the myocardium and liver. This allows for better visualization of deep mammary tissue without any significant interference from activity present in the thoracic cavity and the other breast. Compton scattering in the breast tissue of gamma rays originating in the heart and liver still provides a significant source of out-of-field activity, but an efficient energy discrimination scheme can reject most of these scattered photons.

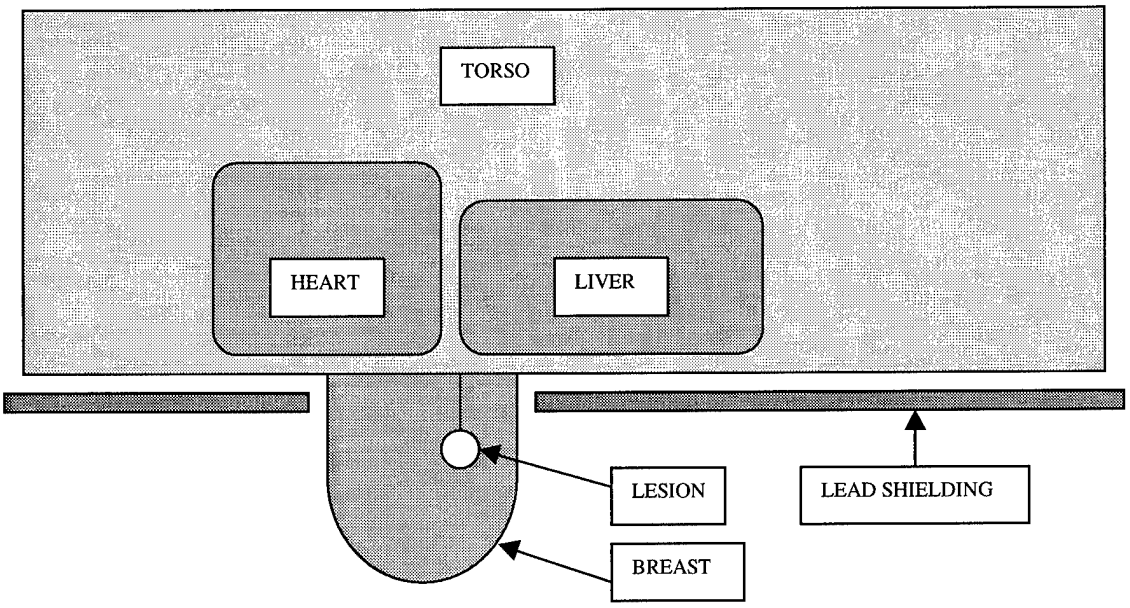

Figure 1. Model of breast and torso.

Two breast phantoms have been constructed. Both phantoms represent a pendant breast. The difference lies in the size. While the base diameter of the breast (nearest the chest wall) is 10 cm in both phantoms, the distance from the base to the tip (the nipple location) is 5 cm in one case and 8 cm in the other. The material used was NCM Clinic D thermoplastic.

Small water-filled plastic spheres will represent lesions within the breast. The sphere diameters range from 5 mm to 30 mm. Each sphere can be attached to a thin plastic rod which, in turn, is mounted on the base of the phantom. The length of the rods ranges from 5 mm to 70 mm. Thus, various sizes and locations of lesions are easily modeled. The breast phantom can also accommodate several lesions (hot and/or cold) at once.

The texture of breast tissue is typically inhomogeneous. Inhomogeneities will be modeled by mixing very small pieces of foam into a gelatinous water-based medium that (along with any spheres representing lesions) will fill the breast phantom.

The torso is modeled by a water-filled plastic storage container (42 cm wide x 65 cm long x 30 cm high). Smaller water-filled and watertight plastic storage containers, representing the heart and liver, will be placed inside the torso phantom. Thus, different levels of radioactivity in the main torso, heart, and liver may be modeled.

OBJECTIVE 2

Task 3. Characterize the response of the small modular gamma cameras.

The characterization of the camera provides an accurate measure of the camera response to a gamma ray incident anywhere on the camera face. The calibration procedure involves stepping a collimated Tc-99m source, oriented such that the beam is normal to the camera face, through a 64 x 64 grid of points on the camera face, and at each point recording the mean camera response to the source activity. The mean camera response consists of the mean signal from each of the photomultiplier tubes (PMT's). The mean signals are obtained by averaging the raw signal data (12,500 events).

The small modular gamma camera contains a 2 x 2 array of square PMT's (56 mm on a side) mounted on a glass light guide (100 mm on a side). The PMT array is centered on the light guide, so that each PMT covers one quadrant (50 mm on a side) of the light guide.

The mean response of a single PMT peaks when the source is directly under the center of the tube and falls off as the source moves away from the center. The decrease in the mean response is not quite radially symmetrical since the PMT is located in one quadrant of the light guide. When the source is under the PMT and near the edges of the camera, the PMT can detect light from scintillation events that scatters off the sides of the scintillation crystal and light guide. Thus, the mean response is slightly different than what it would be if the source were under the central region of the camera.

An example of the normalized mean response of a single PMT, or the "mean detector response function" (mdrf), is shown in Figure 2. The camera face has been subdivided into a 64 x 64 grid of detector pixels (with position indices of 0...63 on each side). Since the PMT's are arranged in a symmetric 2 x 2 array, the mdrf contour of each tube is similar but just rotated such that the peak is in a different corner.

A common diagnostic plot is a particular diagonal of the mdrf contour. The diagonal chosen is the one, which passes through the location of the center of the PMT. An example is plotted in Figure 3. The data represents the diagonal running from (0,0) to (63,63) in the mdrf contour shown in Figure 2.

The "point array" is also a useful tool for examining the performance -- spatial resolution, in particular -- of the modular gamma camera. The data for a point array is obtained by stepping a collimated source through an 8 x 8 grid of locations on the camera face, recording the tube signals for 12,500 events (the same as an mdrf) at each location, and processing the signals with scatter rejection and position estimation software. The resulting point array image is a histogram of the estimated locations where unscattered gamma rays struck the camera face. Since the image is essentially an array of points, both the spatial resolution of the camera and the performance of the position estimation software can be qualitatively analyzed. An example of a real point array is shown in Figure 4. The central region of the camera exhibits much better performance than the edges and corners. Each pixel in the image represents a 1.5625 mm x 1.5625 mm region on the camera face, and the diameter of the collimated source beam is about 2 mm. Thus, the locations of nearly all events, which occur within the central region of the camera, are correctly estimated to within the width of about one pixel.

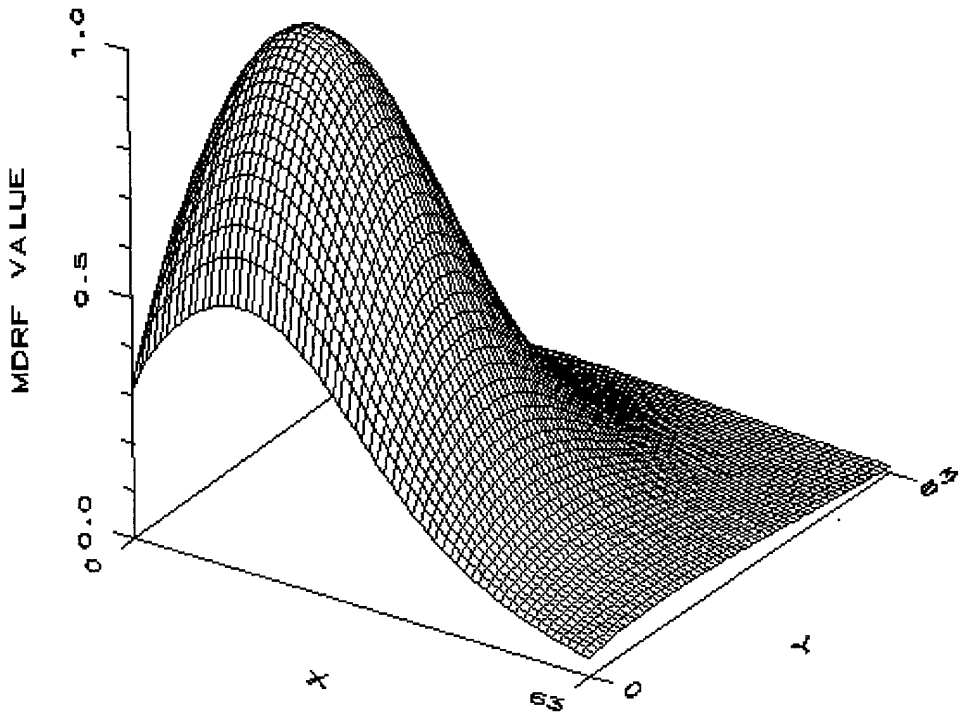

Figure 2. Mean detector response function (mdrf) of a single PMT.

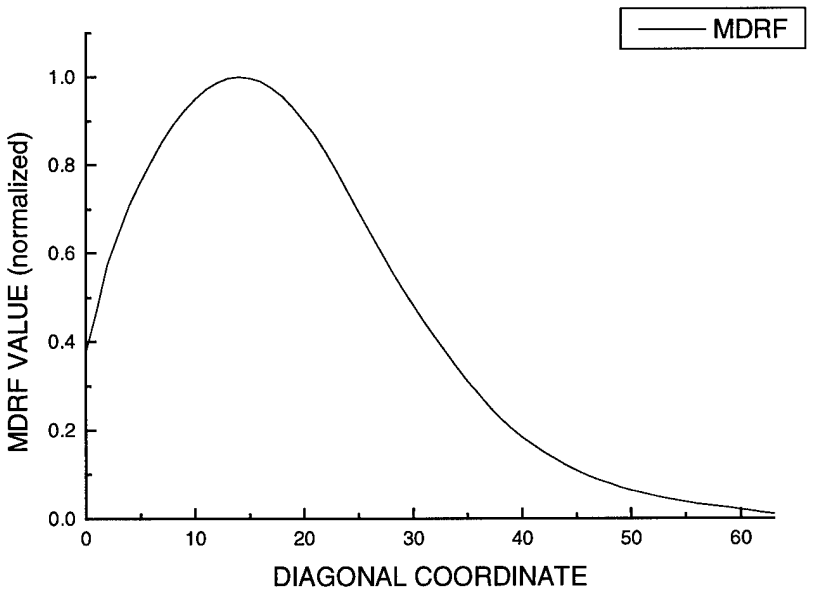

Figure 3. Diagonal of mdrf contour in Figure 2.

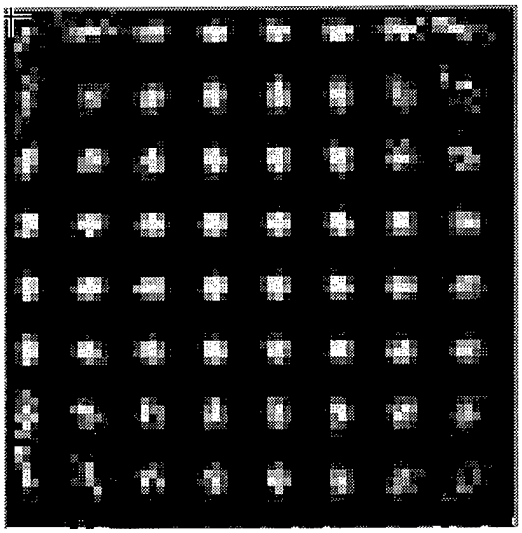

Figure 4. Sample of a real 8 x 8 point array.

An optical model was developed to predict the mean response of the smaller modular gamma camera. The model could then be used in simulations to test and optimize various parameters of camera design and/or performance which, if done in the laboratory, would have consumed considerable time and expense.

The model, taking into account the physical and optical properties of the camera components, performs radiometric calculations to determine the fate of all the light emitted by a scintillation event. In particular, the amount of light detected by each PMT is calculated. Thus, the model estimates the mean response of any PMT to a scintillation event located anywhere within the scintillation crystal.

The optical model, for a given set of parameters, generates mdrf contours like that in Figure 2. The parameters include defined physical quantities -- dimensions, refractive indices, etc. -- and estimated physical quantities -- reflectances and transmittances, surface roughness characteristics, etc.

For the case of the small modular gamma camera, the diagonal of a model mdrf contour is shown in Figure 5 along with the real mdrf diagonal from Figure 3 for comparison. The model diagonal comes very close to matching the real diagonal. The rate of falloff of the mdrf plot (to the right of the peak, in particular) depends, in part, on the amount and type of scattering which occurs at the top and bottom surfaces of the scintillation crystal, both of which are quite rough. Several models of the scattering process have been proposed and incorporated into the model. The model plot in Figure 5 represents the scheme that not only makes reasonable physical sense but also produces results closely matching the mdrf data from a real camera. The rates of falloff are not identical, indicating that the scatter -- and other factors as well -- have not been completely characterized.

The optical model, given the modeled mean responses and a data set of 12,500 randomly generated events (each event consists of four random PMT signals) per grid point, can generate corresponding point arrays like that in Figure 4. For the small modular gamma camera, the model point array is shown in Figure 6 (right hand side) along with the

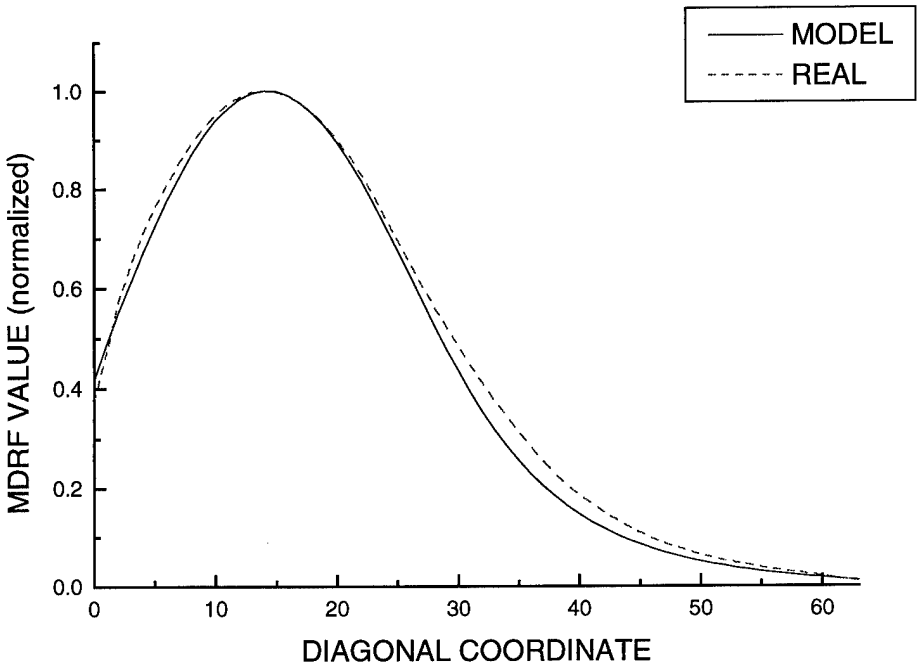

Figure 5. Comparison of real mdrf diagonal to model mdrf diagonal.

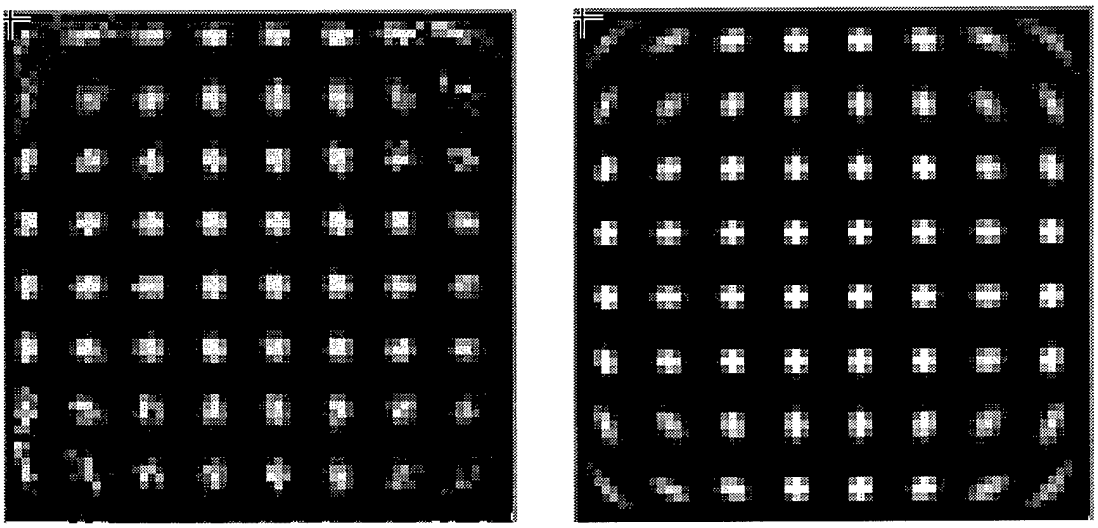

Figure 6. Comparison of real point array (on left) to model point array (on right).

real point array from Figure 4 (left-hand side) for comparison. The model point array is quite similar to the real point array. The performance in the central region of the camera face is comparable to that of the real camera and deteriorates as the source moves near the edges and corners. In the corners, the increase in number of possible estimated locations (illustrated by the "smearing" of the "points") is confirmed. The real point array indicates that such an effect is occurring, but the actual shape of the locus of points is not clear. Part of the reason for this decrease in performance in the corners is poorer scatter rejection. While easily rejected in the central region of the camera, scattered photons are harder to detect and reject at the edges of the camera. Thus, they tend to build up near the edges. This phenomenon has been termed "scatter packing" and was seen by Conrad *et al* [21]. Another part of the reason for this decrease in performance in the corners is that the gradients of the mdrf curves for all but the closest PMT are very shallow at these locations. The position estimation scheme works much better when the gradients of the mdrf contours of at least two tubes are relatively steep at the particular location. The combination of poorer scatter rejection and position estimation near the corners is predicted by the model point array and confirmed by the real point array.

Thus, as shown by comparisons between both the mdrf diagonal plots and the point arrays, the optical model is generating mean responses of the small modular gamma camera comparable to the real modular camera.

Task 4. Characterize the response of the large modular gamma cameras.

An estimated mean response of the proposed large modular gamma camera, consisting of a 3 x 3 array of photomultiplier tubes (PMT's), a fused quartz light guide (15 cm on a side), and a NaI(Tl) scintillation crystal (15 cm on a side), has been generated. The method of doing so, however, differed from that outlined in the original proposal. The original proposal called for a simple extrapolation of known laboratory data from a smaller camera using a 2 x 2 array of PMT's. Initial work on the extrapolation, however, quickly indicated that such an approach was neither practical nor capable of yielding good estimates of the mean responses for a larger camera. So the effort on this task shifted to developing a theoretical method of estimating the mean responses.

An optical model, quite similar to the model of the small camera, was developed to predict the mean response of the larger modular gamma camera. Since a prototype has not been built yet, the model will be used in simulations to test and optimize various parameters of camera design and/or performance which, if done in the laboratory, would consume considerable time and expense.

The optical model, for a given set of parameters, generates mdrf contours similar to that in Figure 2 but over a larger area. In particular, while the mdrf contour for a small camera is defined on a 64 x 64 grid, the contour for a large camera requires a 96 x 96 grid. Also, while the shape of the mdrf contour is quite similar to that of the small camera, its exact shape and the location of its peak value will depend on whether the tube in question is in a corner, on a side, or in the middle of the camera. As shown in Figure 7, the nine tubes on a large camera consist of four corner tubes, four side tubes, and one center tube.

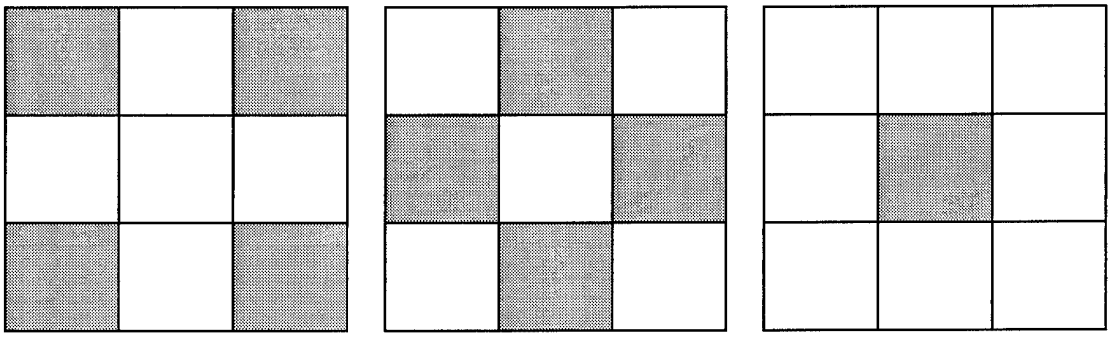

(a) **(b)** **(c)**

Figure 7 . Location of (a) corner, (b) side, and (c) center tubes.

The diagonal of the model mdrf contour for a corner tube is plotted in Figure 8. The basic difference between it and the diagonal of a corner tube of a small camera (see Figure 3) is that it has a longer "tail" (diagonal coordinates 64-95).

The optical model, given the modeled mean responses and a data set of 12,500 randomly generated events (each event consists of four random PMT signals) per grid point, generated the 12 x 12 point array shown in Figure 9. Similar to an 8 x 8 point array

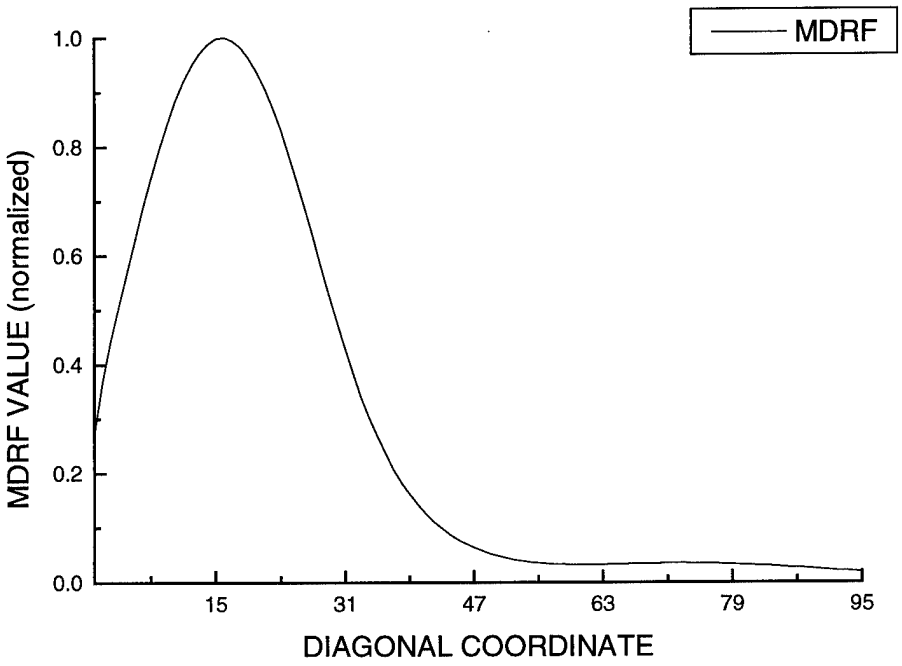

Figure 8. Diagonal of model mdrf contour for a large camera.

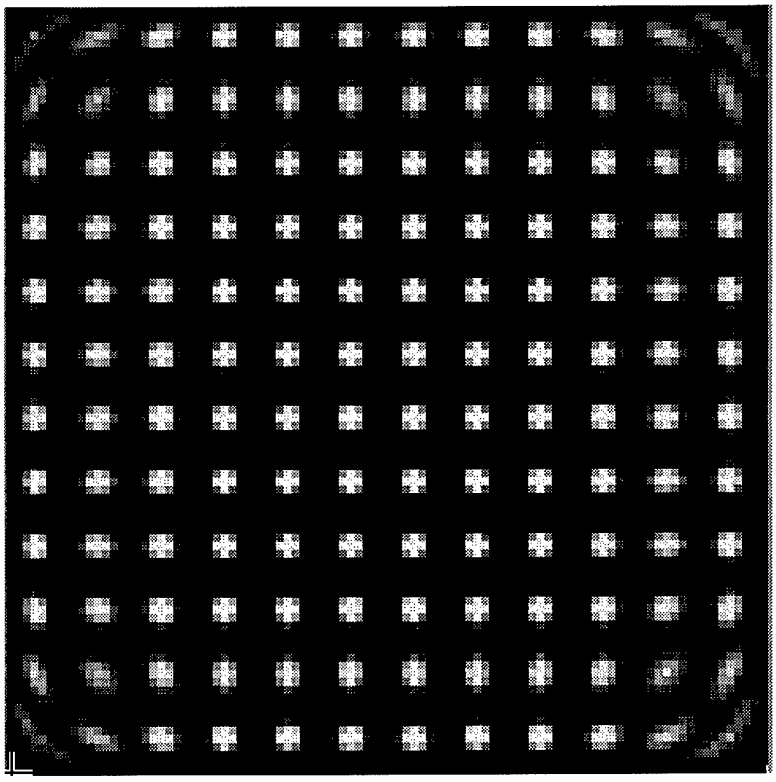

Figure 9. Model point array for a large camera.

for a small camera, performance in the central region of the camera face is relatively good but degrades near the edges and corners.

Task 5. Optimize the geometry of the system configuration.

The purpose of the optimization of the geometry of the system configuration was to define the position and field of view of each camera, the number, size, and arrangement of pinhole apertures, and the magnification of the object.

The optimization is not complete. In fact, such optimization is a process that goes hand in hand with determining how well the system can detect various types of lesions within a breast. Thus, the optimization will continue as the system capabilities evolve.

The optimization to date involves the (a) position and (b) field of view of the small cameras. With respect to position, the small cameras were originally pointed slightly inward at the breast as shown in Figure 10. They have now been repositioned such that they are parallel to the patient's body as shown in Figure 11. Although the distance has yet to be defined, the cameras will be closer to the breast than before. With respect to field of view, the pinhole apertures have been replaced with parallel-hole collimators. Thus, the field of view is no longer a cone which includes the breast and part of the thoracic cavity behind it (see Figure 10) but rather a straight-ahead view, parallel to the body, that includes only the breast (see Figure 11).

Both of these changes work together to help eliminate the detection of unwanted intrathoracic activity. A significant problem in mammoscintigraphy is the location of the breast. The breast is located very close to the heart and liver, organs that exhibit high uptakes of Tc-99m Sestamibi. The system field of view should, if possible, exclude these organs and any other part of the body that acts as a source of unwanted activity. The cameras will still detect some activity from the heart and liver, in the form of gamma rays Compton scattered within the breast tissue, but the system has a better chance of distinguishing them as scatter and rejecting them.

The object magnification is automatically affected by the above changes. Since parallel-hole collimators will be used, the object magnification is necessarily 1.0.

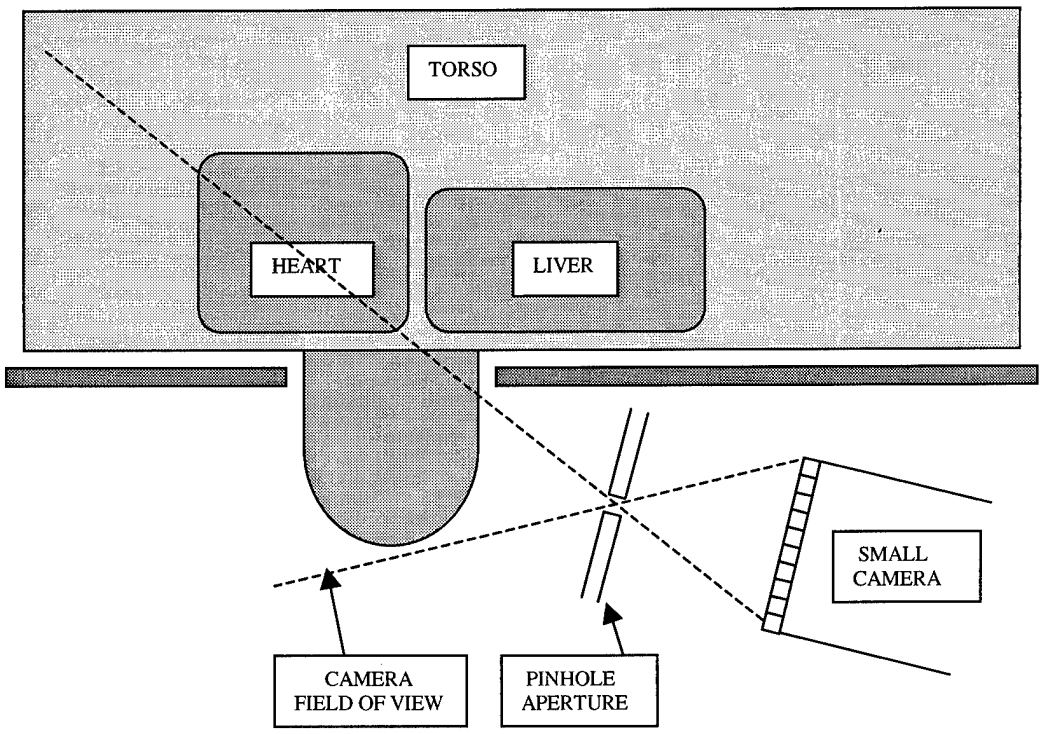

Figure 10. Original position and field of view of a small camera.

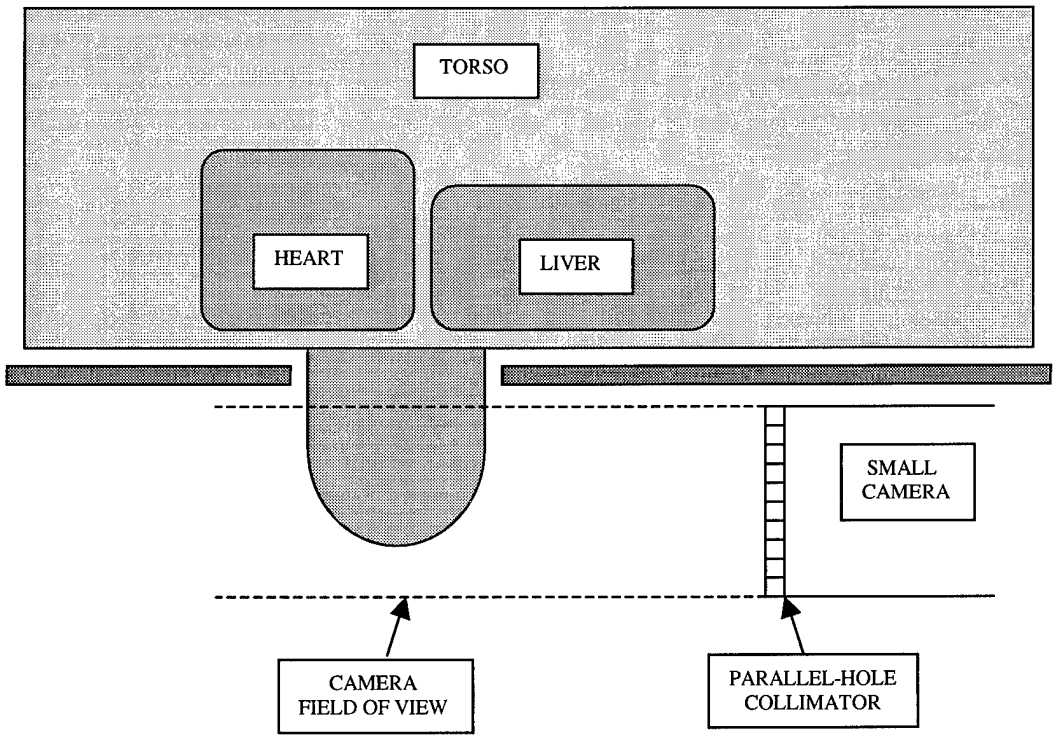

Figure 11. Current position and field of view of a small camera.

CONCLUSIONS

Task 1. Characterize the expected radiotracer activity within the breast.

In clinical studies a standard injection of Tc-99m Sestamibi into a patient contains 20 mCi of activity. A minute fraction of this activity ends up in the breasts. The estimated percentage of the original injected activity taken up by a single breast of average mass (410 g, according to the Cristy-Eckerman model) is about 0.08 %, which corresponds to about 16 uCi. The estimated activity per unit mass of normal breast tissue is about 43 dpm/mg.

The uptake of Tc-99m Sestamibi by abnormal types of tissue (relative to normal breast tissue) varies. Fatty tissue tends to take up about the same amount as normal tissue. Malignant tumors, on the other hand, typically exhibit high relative uptakes. The degree of uptake appears to vary significantly with the histological type of the tumor and not the histological grade. For example, ductal and lobular carcinomas exhibit a relative uptake ratio of nearly 6:1 and fibroadenomas nearly 3:1. Other types of abnormalities, such as inflammations, fibrocystic disease, and sclerosing adenoses, have been known to occasionally take up a significant amount of Tc-99m Sestamibi, but the uptake is not consistently high. The relative uptake ratio can range from 1:1 to 3:1. Some abnormalities, such as cysts, benign tumors, and epithelial hyperplasia, typically exhibit low relative uptakes, or uptakes similar to normal breast and fatty tissue.

Task 2. Build a realistic model of the human breast and adjacent chest wall.

A model of a female torso containing breast, heart, and liver phantoms has been constructed. The breast phantom comes in two sizes and is capable of holding several hot and/or cold lesions. The lesions are modeled by water-filled plastic spheres of various diameters and can be located anywhere within the breast phantom. The torso model represents a human torso from the shoulders to the hips. Both heart and liver phantoms can be placed inside it. Thus, specific levels of radioactivity in the main torso, heart, and liver may be modeled.

The complete model represents a prone female with one pendant breast. Several recent clinical imaging studies have favored the prone position (over the erect position) because it allows for better visualization of deep mammary tissue without any significant interference from activity present in the thoracic cavity.

Task 3. Characterize the response of the small modular gamma camera.

The mean response of the small modular gamma cameras has been characterized. An optical model was developed which provides an estimate of the camera response to a gamma ray incident anywhere on the camera face. The data generated by the model nearly matches the data obtained from a real camera in the laboratory.

The optical model, taking into account the physical and optical properties of the camera components, performs radiometric calculations to determine the fate of all of the light emitted by a scintillation event. In particular, the amount of light detected by each

photomultiplier tube is calculated, so the mean response of any photomultiplier tube to a scintillation event located anywhere within the scintillation crystal can be estimated.

Task 4. Characterize the response of the large modular gamma camera.

The estimated mean response of the large modular gamma camera has been characterized. An optical model, very similar to the model of the small camera, was developed which provides an estimate of the camera response to a gamma ray incident anywhere on the camera face. No comparison to real data can be made since a large camera has not been built yet. Given that the small and large cameras are so similar in design, the assumption is that the model, which worked so well for the small camera, will also work well for the large camera.

Task 5. Optimize the geometry of the system configuration.

Parameters to be optimized include the position and field of view of each camera, the number, size, and arrangement of the pinhole apertures, and the magnification of the object. The optimization, not complete at this point, will continue to evolve with the system development.

A major concern in breast imaging is out-of-field activity from the heart and liver, both of which take up significant amounts of Tc-99m Sestamibi. The original design of the system called for each small camera to have a roughly conical field of view that included the whole breast and, as a result, part of the thoracic cavity. The decision was made to eliminate as much intrathoracic activity as possible from the field of view by modifying the position and field of view of the small cameras. With respect to position, instead of pointing slightly inward towards the chest cavity, the small cameras are now aligned parallel to the torso. With respect to field of view, instead of using pinhole apertures, the small cameras will be outfitted with parallel-hole collimators, so each will look straight ahead. The object magnification, a casualty of this decision, will be restricted to 1.0 because of the parallel-hole collimators.

REFERENCES

[1] Cristy M, Eckerman K. Specific absorbed fraction of energy at various ages from internal photon sources. ORNL/TM-8381 V1-V7, Oak Ridge, Tenn., 1987, Oak Ridge National Laboratory.

[2] Maublant J, de Latour M, Mestas D, Clemenson A, Charrier S, Feillel V, Le Bouedec G, Kaufmann P, Dauplat J, Veyre A. Technetium-99m Sestamibi uptake in breast tumor and associated lymph nodes. *J Nucl Med* 1996 (37) 922-925.

[3] Personal communication. Maublant, Jean. Department of Nuclear Medicine, Centre Jean Perrin, 63011 Clermont-Ferrand, France. January 1998.

[4] Wackers F, Berman D, Maddahi J, Watson D, Beller G, Strauss H, Boucher C, Picard M, Homan B, Fridrich R, Inglese E, Delaloye B, Bischof-Delaloye A, Camin L, McKusick K. Technetium-99m hexakis 2-methoxyisobutylisonitrile: human biodistribution, dosimetry, safety, and preliminary comparison to thallium-201 for myocardial perfusion imaging. *J Nucl Med* 1989 (30) 301-311.

[5] Cristy M, Eckerman K. Specific absorbed fraction of energy at various ages from internal photon sources. ORNL/TM-8381 V1-V7, Oak Ridge, Tenn., 1987, Oak Ridge National Laboratory.

[6] Ambrus E, Rajtar M, Ormandi K, Sera T, Toszegi A, Lang J, Pavics L, Csernay L. Value of 99m-Tc MIBI and 99m-Tc(V) DMSA Scintigraphy in Evaluation of Breast Mass Lesions. *Anticancer Research* 1997 (17) 1599-1606.

[7] Trojani M. A color atlas of breast histopathology. J.B. Lippincott Co. Philadephia 1991.

[8] Mangkharak J, Patanachak C, Podhisuwan K, Pleehachinda R. The evaluation of combined scintimammography and tumor markers in breast cancer patients. *Anticancer Research* 1997 (17) 1611-1614.

[9] American Joint Committee on Cancer: Manual Staging of Cancer. 4th Edition. J.B. Lippincott. Philadelphia 1992. Pp.149-154.

[10] Buscombe J, Cwikla J, Thakrar D, Hilson A. Uptake of Tc-99m MIBI related to tumor size and type. *Anticancer Research* 1997 (17) 1693-1694.

[11] Chen S, Yin Y, Chen J, Sun X, Xiu Y, Liu W, Liu M, Zhu W, Zhang Y. The usefulness of Technetium-99m-MIBI scintimammography in diagnosis of breast cancer: Using surgical histopathologic diagnosis as the gold standard. *Anticancer Research* 1997 (17) 1695-1698.

[12] Carril J, Gomez-Barquin R, Quirce R, Tabuenca O, Uriarte I, Montero A. Contribution of 99mTc-MIBI scintimammography to the diagnosis of non-palpable breast lesions in relation to mammographic probability of malignancy. *Anticancer Research* 1997 (17) 1677-1682.

[13] Chen S, Yin Y, Chen J, Sun X, Xiu Y, Liu W, Liu M, Zhu W, Zhang Y. The usefulness of Technetium-99m-MIBI scintimammography in diagnosis of breast cancer: Using surgical histopathologic diagnosis as the gold standard. *Anticancer Research* 1997 (17) 1695-1698.

[14] Khalkhali I, Cutrone J, Mena I, Diggles L, Venegas R, Vargas R, Jackson B, Klein S. Technetium-99m-Sestamibi scintimammography of breast lesions: Clinical and pathological follow-up. *J Nucl Med* 1995 (36) 10:1784-1789.

[15] Palmedo H, Schomburg A, Grunwald F, Mallmann P, Krebs D, Biersack H. Technetium-99m-MIBI scintimammography for suspicious breast lesions. *J Nucl Med* 1996 (37) 4:626-630.
[16] Scopinaro F, Schillaci O, Ussof W, Nordling K, Capoferro R, de Vincentis G, Danieli R, Ierardi M, Picardi V, Tavolaro R, Colella A. A three center study on the diagnostic accuracy of 99mTc-MIBI scintimammography. *Anticancer Research* 1997 (17) 1631-1634.
[17] Taillefer R, Robidoux A, Lambert R, Turpin S, Laperriere J. Technetium-99m-Sestamibi prone scintimammography to detect primary breast cancer and axillary lymph node involvement. *J Nucl Med* 1995 (36) 10:1758-1765.
[18] Villanueva-Meyer J, Leonard Jr M, Briscoe E, Cesani F, Ali S, Rhoden S, Hove M, Cowan D. Mammoscintigraphy with technetium-99m-Sestamibi in suspected breast cancer. *J Nucl Med* 1996 (37) 6:926-930.
[19] Dupont W, Page D. Risk factors for breast cancer in women with proliferative breast disease. *N Engl J Med* 1985 312:146-151.
[20] Jenses R, Page D, Dupont W, Rogers L. Invasive breast cancer risk in women with sclerosing adenosis. *Cancer* 1989 64:1977-1983.
[21] Conrad B, Klingenbeck-Regn. Scatter sensitivity of modular gamma camera. Siemen's technical report. 1991.